Supporting information

Interaction between Carbon Dots from folic acid and their cellular receptor: a qualitative physicochemical approach.

Erika Adhel,[a] Nguyêt-Thanh Ha Duong,[a] Thi Huyen Vu,[b] Dario Taverna,[c] Souad Ammar [a] and Nawal Serradji. [a,*]

[a] Université Paris Cité, CNRS, ITODYS, F-75013 Paris, France.

[b] University of Engineering and Technology, Vietnam National University, Hanoi (VNUH), Vietnam.

[c] Sorbonne Université, CNRS, IMPMC, F-75005 Paris, France.

*corresponding author: serradji@u-paris.fr; Phone number: +33 1 57278883; Fax number: +33 1 57277263

Table of contents

1. **CD_{FAs} characterization**

The hydrodynamic diameter of purified CDs_{FA} was measured in both milli-Q water and phosphate buffer solution. Statistical analysis of particle size, extracted from DLS data, indicates a size distribution of 2–6 nm whatever the medium. Typically, in milli-Q water, the particle diameter ranges from 2.7 to 5.6 nm with an average diameter of 3.6 ± 0.4 nm (Fig. S1a), in agreement with the results of Bunhia *et al*. (3.5 ± 0.1 nm).

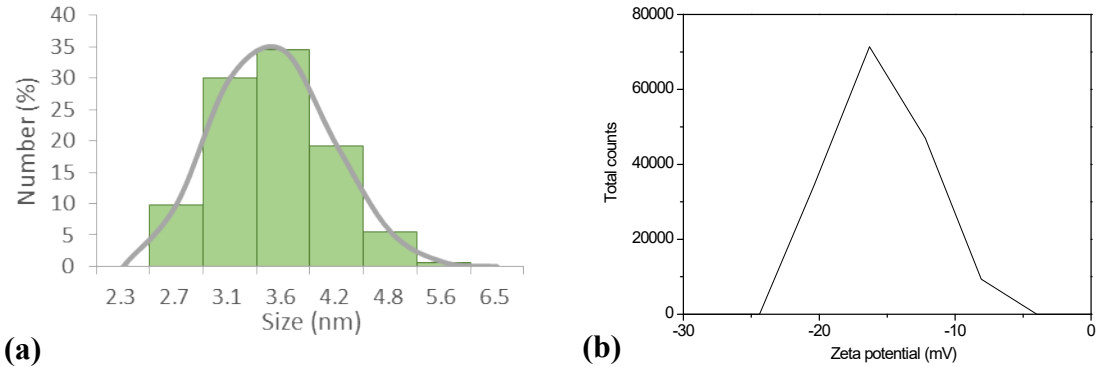

Fig. S1 (a) Hydrodynamic size distribution of CDs_{FA} at 15 µg/mL in aqueous solution; (b) Zeta potential of CDs_{FA} measured on a 1 mg/mL suspension in milli-Q water.

The zeta potential (ζ) value is an indication of the stability of an aqueous dispersion of NPs. This measurement is directly related to the charges of groups attached to the NP surface. Since these groups depend on the pH of the solution, the zeta potential can be changed by varying the pH to alter or improve the stability of the suspension. The purpose of this measurement was to evaluate the stability of our CDs_{FA} first in milli-Q water, and then in 20 mM phosphate buffer at pH 7.4, in which we studied the interaction with the target protein of interest. In these media, CDs_{FA} have zeta potentials of -16.3 and -19.1 mV, respectively, which means that the particles produced are globally negatively charged at their surface, with acceptable colloidal stability (Fig. S1b).

The morphology of these particles was then studied by TEM, combining HRTEM, HAADF and STEM-EELS analyses. STEM-HAADF images show nearly spherical, almost non-aggregated, contrasted objects less than 10 nm in diameter (Fig. S2a). The absence of crystallinity highlights the fact that these particles are amorphous (Fig. S2b), one morphology already described for the CDs.[1] This assumption is also suggested by the general shape of the carbon K-edge in the CDs_{FA}' EELS spectra (Fig. S2c). At this stage of the analysis, it is hard to

confirm unambiguously such a conclusion since CDs signal, in both the electron diffraction and the EELS data, is superimposed with that of the dominant substrate signature. Nevertheless, EELS data establish that CDs_{FA} as mainly carbon made objects, containing also a certain amount of nitrogen.

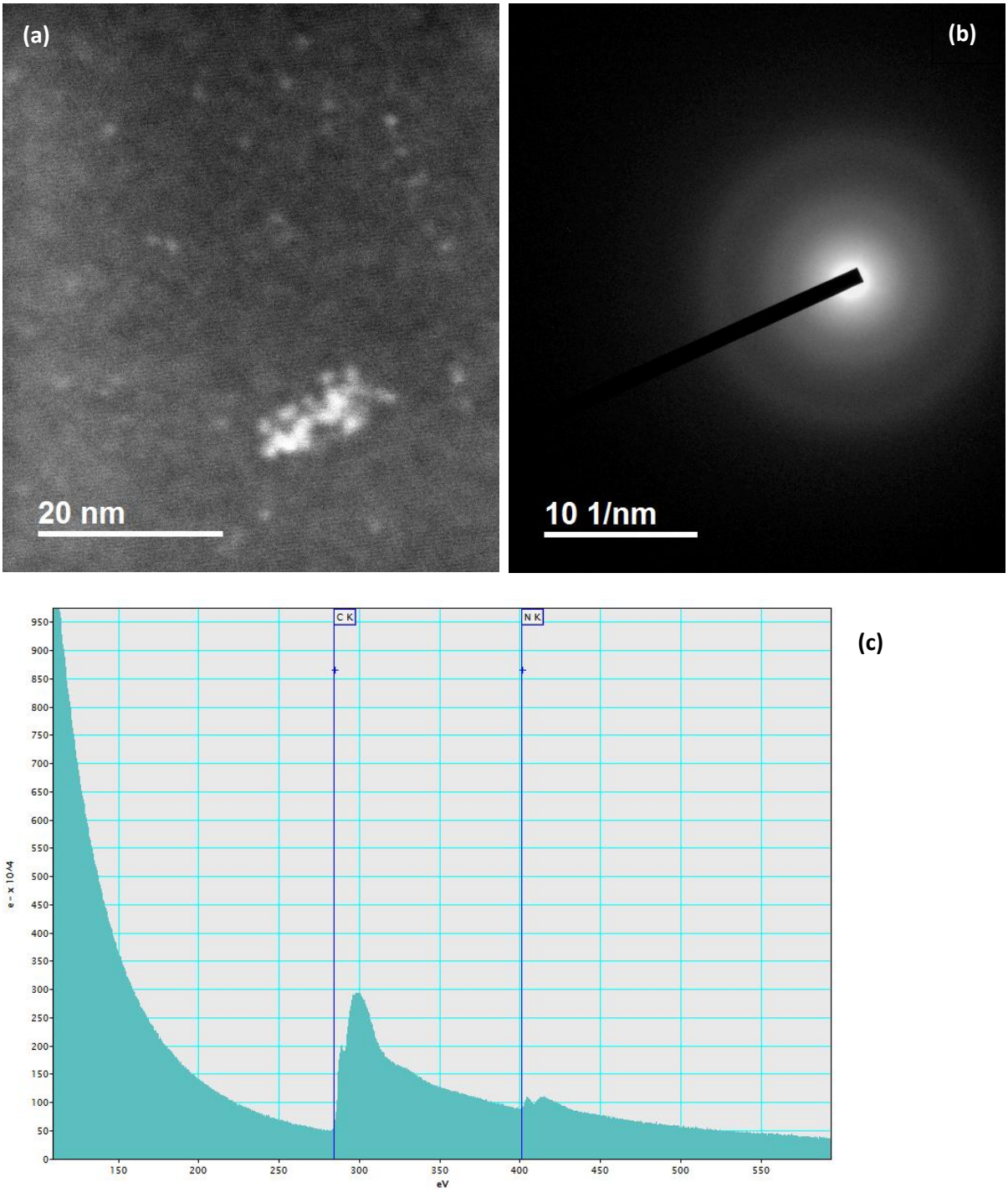

Fig. S2 (**a**) HAADF-STEM image of an assembly of CDs_{FA}; (**b**) TEM electron diffraction pattern of a region containing CDs_{FA} showing no evidence of crystalline structure; (**c**) Typical electron energy-loss spectrum of CDs_{FA} region.

XPS experiments on fresh CDs_{FA} powder mounted on carbon tape (Fig. S3a) confirmed that the particles consist mainly of carbon (60.3%), and non-negligible amounts of nitrogen (18.7%) and oxygen (19.1%). Usually XPS measurements are assumed to be representative of the extreme surface of the analyzed matter, but since the average size of the studied CDs is of some nanometers in diameters only, one may assume that the XPS results are representative of the whole particle volume.

Specifically, carbon is of several types: C=C at 284.41 eV, C–C at 285.53 eV, C–N/C–O at 287.60 eV and C=O at 288.78 eV (Fig. S3b). The first, the strongest C1s signal, is attributed to the particle core, while the others, lower in intensity, are assumed to be due to superficial nitrogen- and oxygen-based organic groups, like amino and carboxylic groups. Of course these results do not exclude a certain nitrogen in-volume doping of the carbon based cores, since EELS analysis showed clearly nitrogen signature but not the oxygen one. However, an attentive observation of the high-resolution N1s and O1s spectra suggest that this doping is very weak. Indeed, the N1s signal appears as a broad peak centered at 399.15 eV, only assigned to N–C and N–H (primary/secondary amine) bonding (Fig. S3d), and the O1s signal at 531.03 eV is attributed to organic C-O and C=O groups (Fig. S3c). The superficial heteroatoms (oxygen and nitrogen) are probably responsible for the negative surface charge measured above.

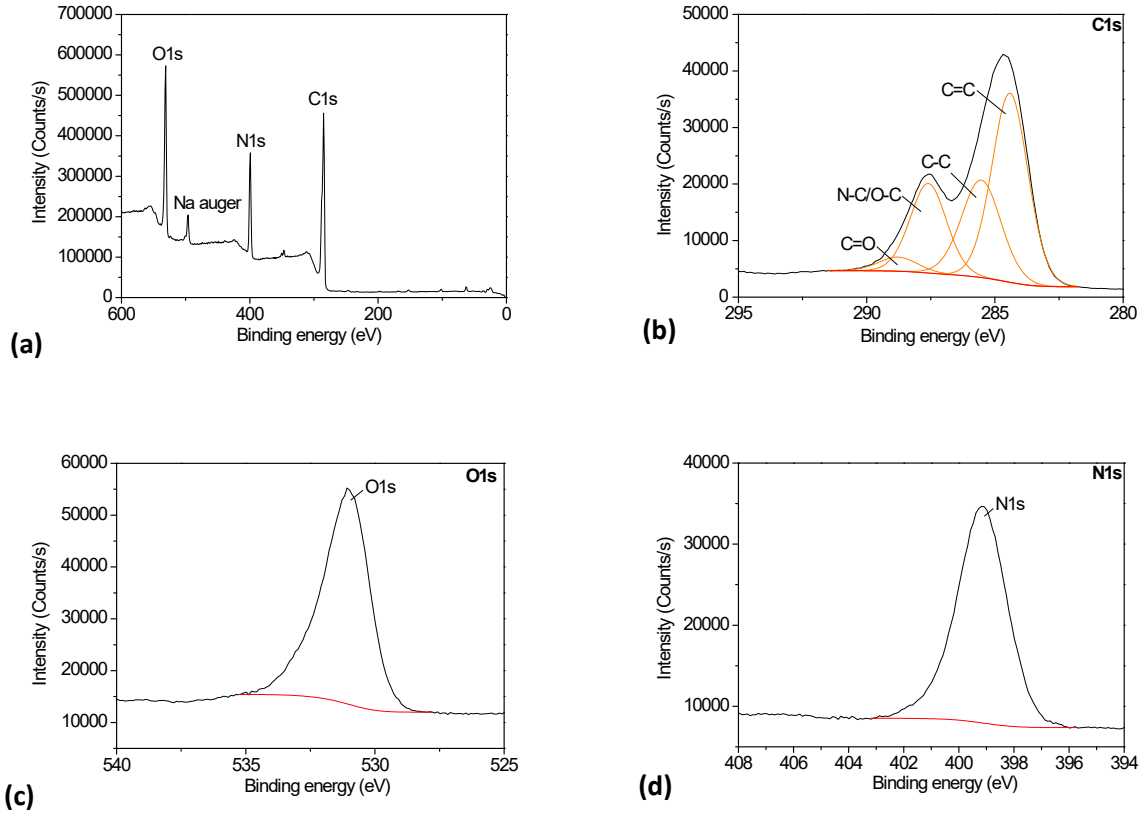

Fig. S3 (**a**) Survey XPS spectra for CDs_{FA}. (**b, c, d**) High-resolution C1s (deconvoluted), O1s and N1s spectra.

FTIR spectra give structural insights about the previously detected organic contents (Fig. S4). Bands centered at 3206, 1679, 1404 and 1288 cm^{-1} were easily identified as the signature of OH/NH, O=C, C–O and C–N vibrations, respectively, confirming the chemical richness of CDs_{FA} surfaces, and all the potentialities for further (bio)chemical functionalization. Comparison with the folic acid spectrum show differences with respect to the functional groups available in the acid, in particular the 3500–2900 cm^{-1} and the 1700–1400 cm^{-1} regions, with a shift from 1692 to 1679 cm^{-1} of the carbonyl stretching vibration.

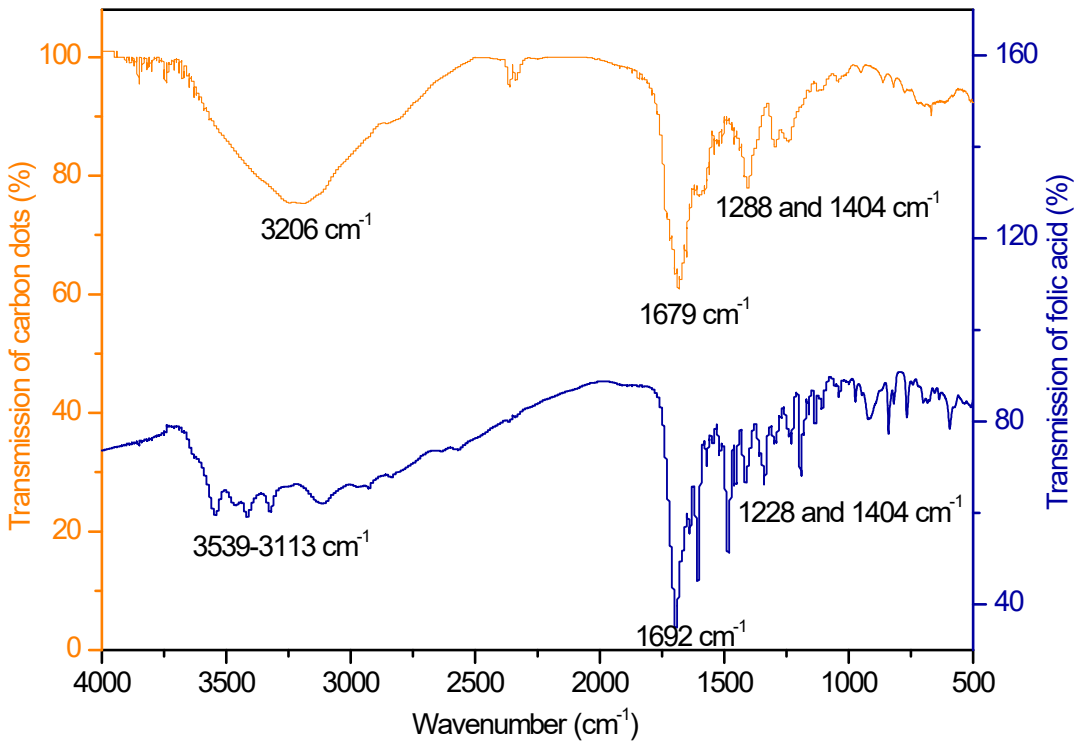

Fig. S4 FT-IR spectrum of CDs_{FA} (orange curve) and FA (blue curve).

2. CDs_{FA} quantum yields

λ excitation (nm)	A_{CD}	A_{S}	I_{CD}	I_{SQ}	Φ_{CD}	Φ_{CDmean}
300	0.100	0.039	$1.197x10^9$	$3.698x10^8$	41	39
320	0.091	0.047	$1.514x10^9$	$6.572x10^8$	38	
340	0.086	0.054	$2.060x10^9$	$1.036x10^9$	36	
350	0.089	0.055	$2.226x10^9$	$1.172x10^9$	37	
355	0.082	0.052	$2.250x10^9$	$1.154x10^9$	39	
360	0.076	0.046	$2.249x10^9$	$1.070x10^9$	40	
370	0.067	0.030	$1.933x10^9$	$7.320\ x10^8$	37	

Table S1 CDs_{FA} quantum yields.

3. FA/FA-R interaction study

The interaction of FA with FBP can be expressed by the following equations 1 and 2:

$$FA + FBP \rightarrow FA - FBP \; where \; Kd = \frac{[FA][FBP]}{[FA - FBP]} \qquad (1)$$

$$\frac{c1}{c3} = 1 + \frac{K_d}{(c2 - c3)} \quad (2)$$

Where $c1,c2,c3$ are the analytical concentrations of FBP, FA and FA-FBP, respectively.

Intrinsic fluorescence was used as a tool to monitor changes in the FBP. At a fixed wavelength (351 nm), the curve representing FA fluorescence intensity as a function of its concentration (c2) follows a quadratic equation (equation 3; Fig. S5) while those of FBP (Fig. S6) and FA-FBP are proportional to their respective concentrations c1 and c3 (equations 4 and 5) in the range studied.

We have:

$$FI(FA) = b * c2^2 + a * c2 \quad (3)$$

$$FI(FBP) = a' * c1 \quad (4)$$

$$FI(FA - FBP) = a'' * c3 \quad (5)$$

where FI is the fluorescence intensity, and a, b, a' and a'' are the experimental coefficients that relate the fluorescence intensity to the analytical concentrations of the species.

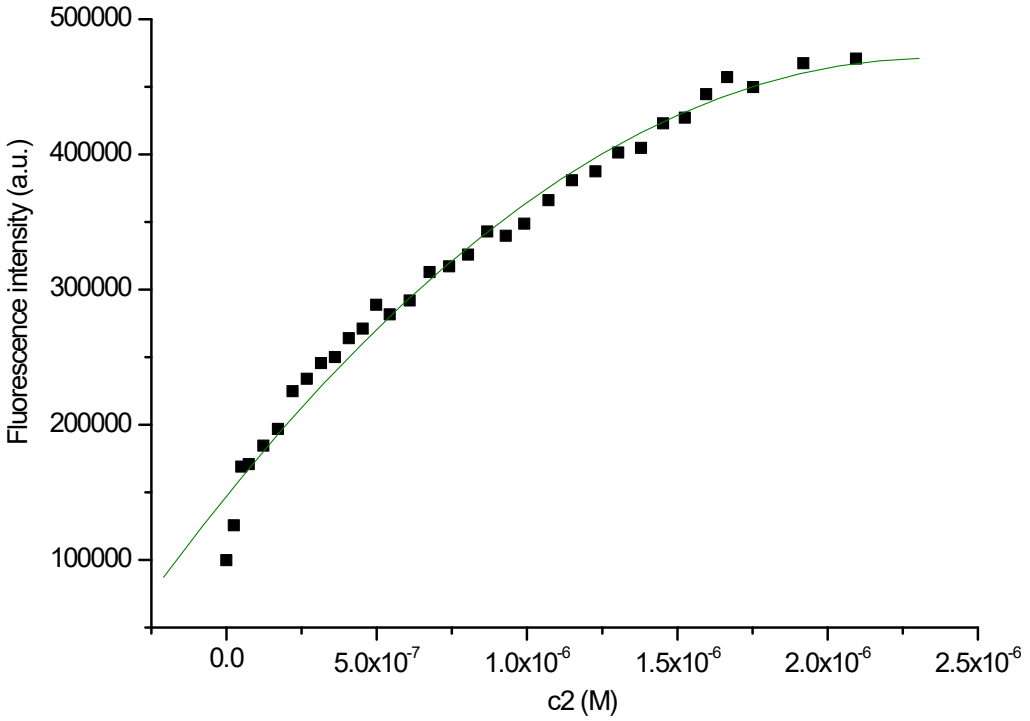

Fig. S5 Fluorescence intensity (FI) of FA as a function of its concentration. Plot of fluorescence intensity against c2. The factors of the polynomial equation *(3)* are: b = (-5.881 ± 0.742)*10^{16}, a = (2.759 ± 0.146)*10^{11} and the constant is (1.474 ± 0.057)*10^{5}. r^2 = 0.982.

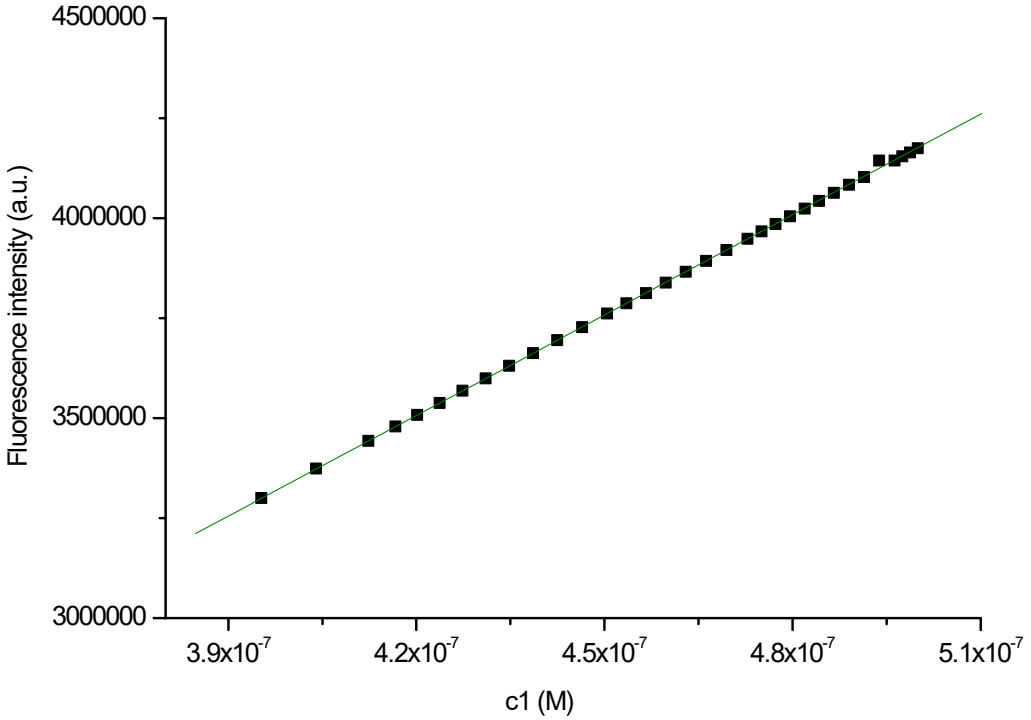

Fig. S6 Fluorescence intensity (FI) of FBP as a function of its concentration. Plot of fluorescence intensity against c1. The intercept is (-1.055 ± 0.951)*10^4, the slope (8.374 ± 0.021)*10^{12} and r^2 = 0.999.

Moreover, the global fluorescence intensity measured is described as follows:

$$FImeasured = FI(FBP) + FI(FA) + FI(FA - FBP) \quad (6)$$

Combination of equations 3-6 leads to:

$$FImeasured = a^{'} * (c1 - c3) + b * (c2 - c3)^2 + a * (c2 - c3) + a^{''} * c3 \quad (7)$$

Under FBP saturation conditions, i.e. at the highest ligand concentration, equation 6 is simplified and gives access to a''. The determination of c3, the FA-FBP complex concentration, is the positive solution of polynomial equation 8 and is obtained after the expression of all the concentrations of equation 7 as a function of c3.

$$b * c3^2 + c3\left(-2 * b * c2 - a - a^{'} + a^{''}\right) + bc2^2 + ac2 + a^{'}c1 - FImeasured = 0 \quad (8)$$

Finally, the slope of the line $c1/c3 = f(1/(c2 - c3))$ (2) provides the K_d value.

Before quantifying this interaction, we demonstrated its existence by the curves presented in Fig. S7.

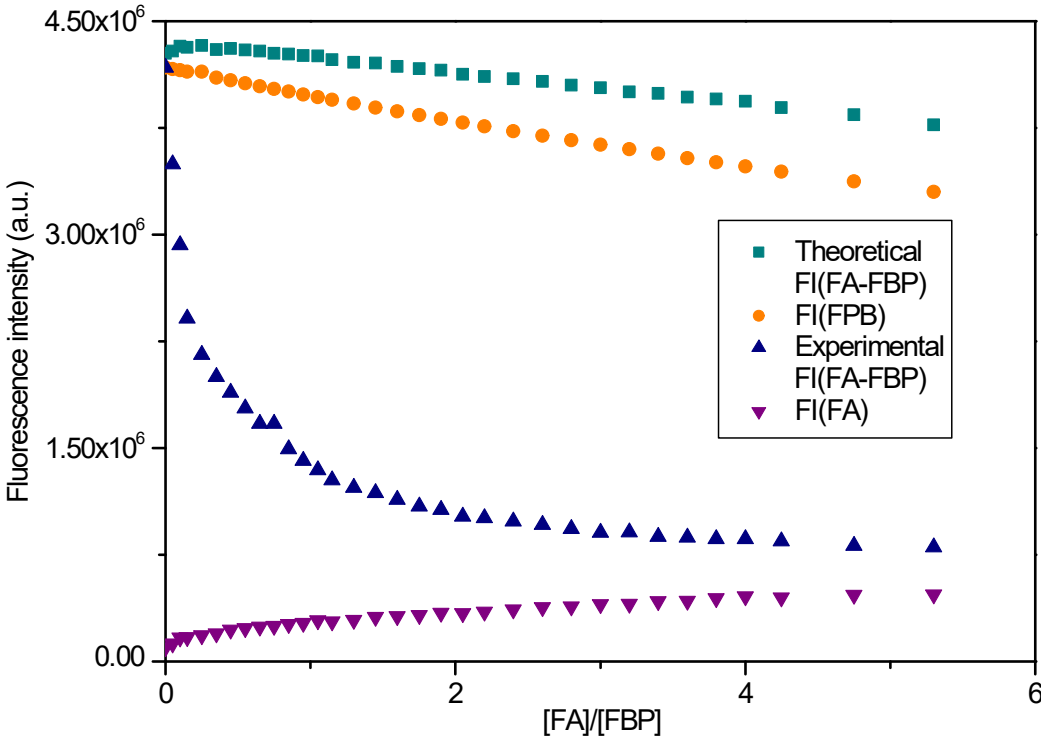

Fig. S7 Fluorescence intensity (FI) variations at 351 nm of FA (purple), FBP (orange), of the FBP in the presence of FA (FA-FBP; blue) and the theoretical sum of FI of FA and FBP (FA-FBP; cyan) as a function of [FA]/[FBP] ratio. λ_{exc} = 280 nm.

In Fig. S7, the difference between the experimental curve (blue curve) and the theoretical curve (green curve) confirms the existence of a FA/FBP interaction.[2] The decrease in the fluorescence intensity of FBP as a function of the gradual addition of FA also demonstrates quenching of the protein fluorescence through an interaction between the two components.

As shown in equation 2, the corresponding slope provides the dissociation constant of this binding $K_d = (9.2 \pm 0.3) * 10^{-8}\, M$ and enables the quantification of this phenomenon (Fig. S8). In addition, the intercept (0.951) obtained is close to the value of 1 expected in equation 2 (Fig. S8). These results confirm that FA binds efficiently to FBP under our experimental conditions.

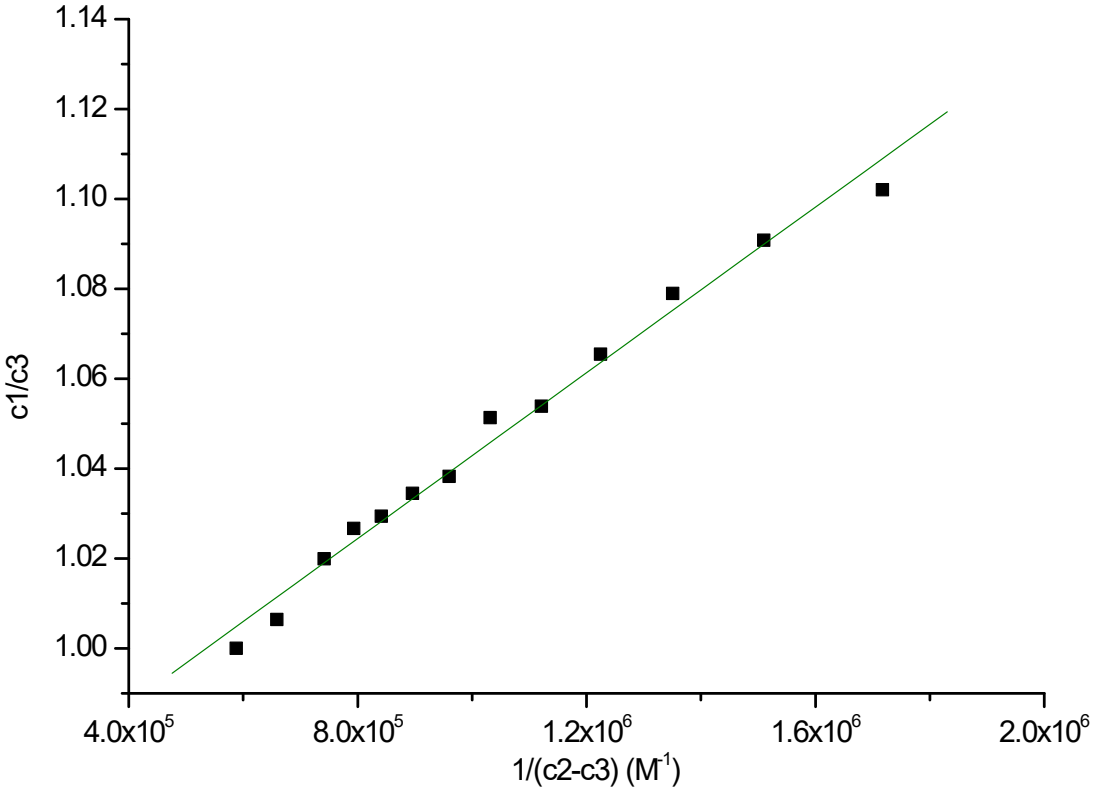

Fig. S8 K_d determination of the FA/FBP interaction. Plot of c1/c3 against 1/(c2-c3). The intercept is (0.951 ± 0.004), the slope (9.2 ± 0.3)*10^{-8} and $r^2 = 0.993$.

4. **PL emission spectra of FBP and CDs_{FA} (Fig. S9) and reverse titration (Fig. S10)**

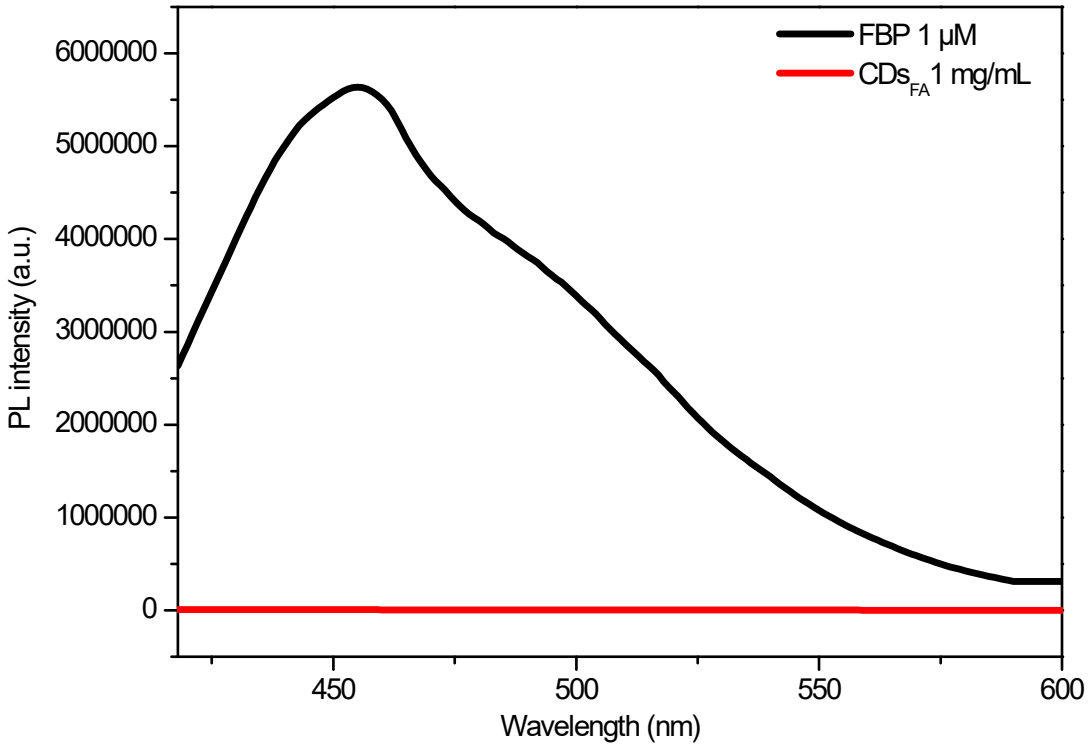

Fig. S9 Photoluminescence (PL) emission spectra of FBP (black curve; 1 µM in a phosphate buffer 20 mM) and CDs_{FA} (red curve; 1 mg/mL in a phosphate buffer 20 mM) recorded with excitation at 350 nm.

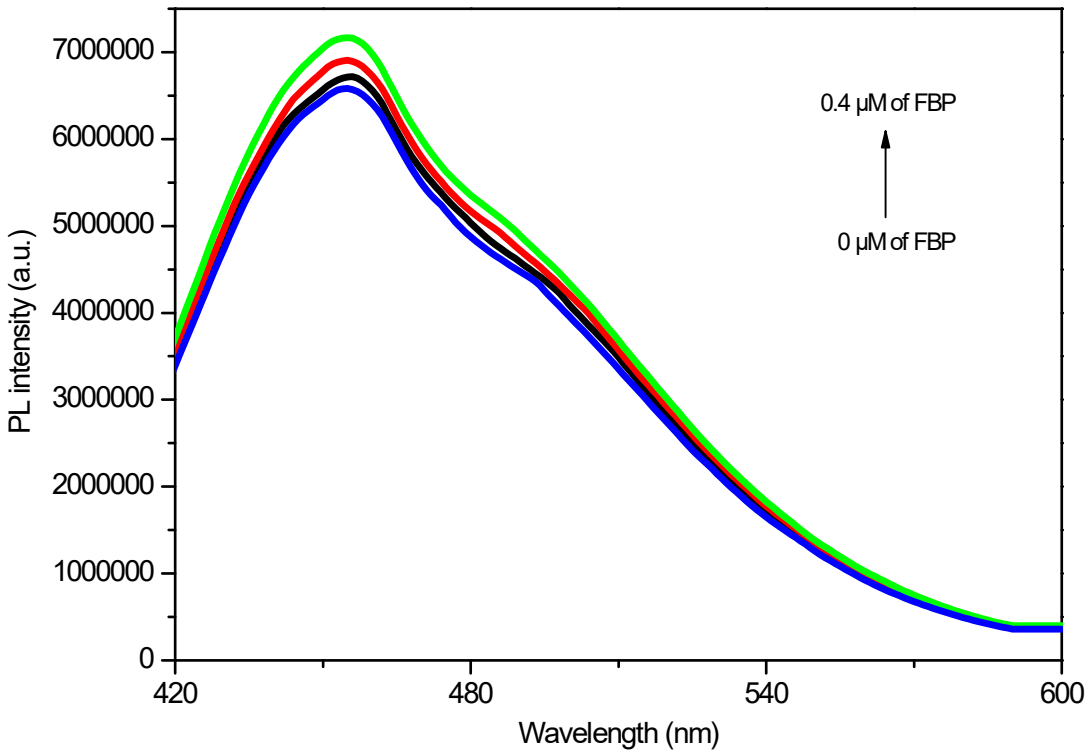

Fig. S10 Photoluminescence (PL) emission spectra of CDs_{FA} upon addition of increasing amounts of FBP recorded with excitation at 350 nm. Experimental conditions: [CDs_{FA}] = 1 mg/mL in a phosphate buffer 20 mM, pH 7.4 at 25 °C. The experiment was performed in duplicate

5. High resolution mass spectroscopy spectrum of CDs_{FA} (ESI^+):

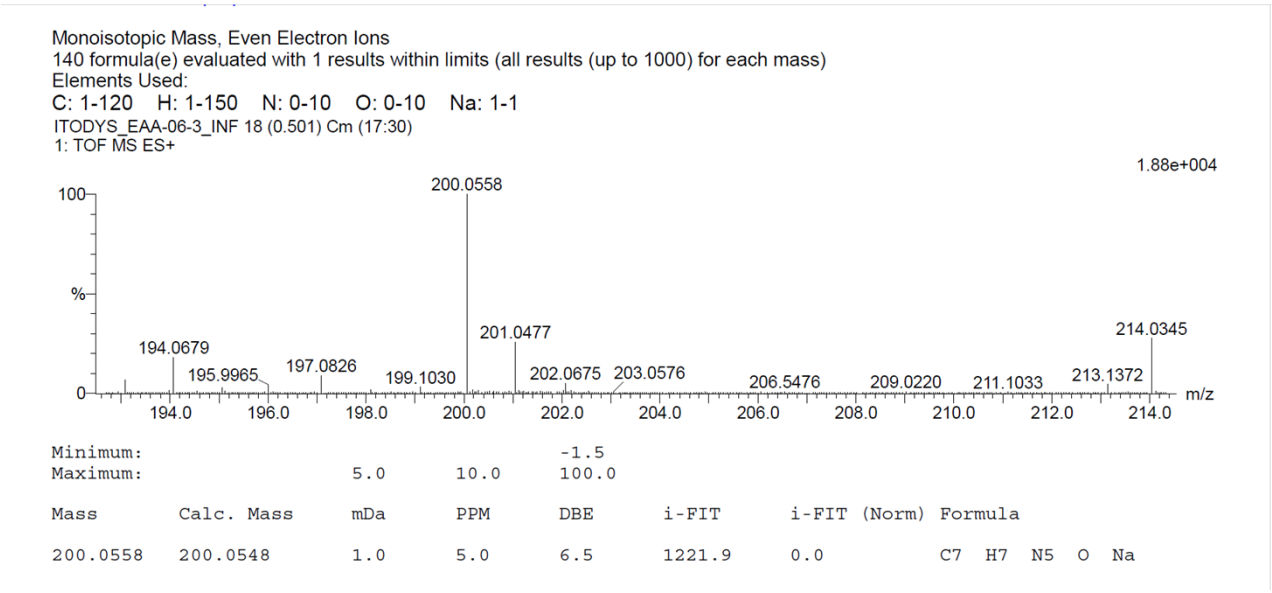

Fig. S11 CDs_{FA} HRMS spectrum.

6. **CDs_{FA}/LF interaction study:**

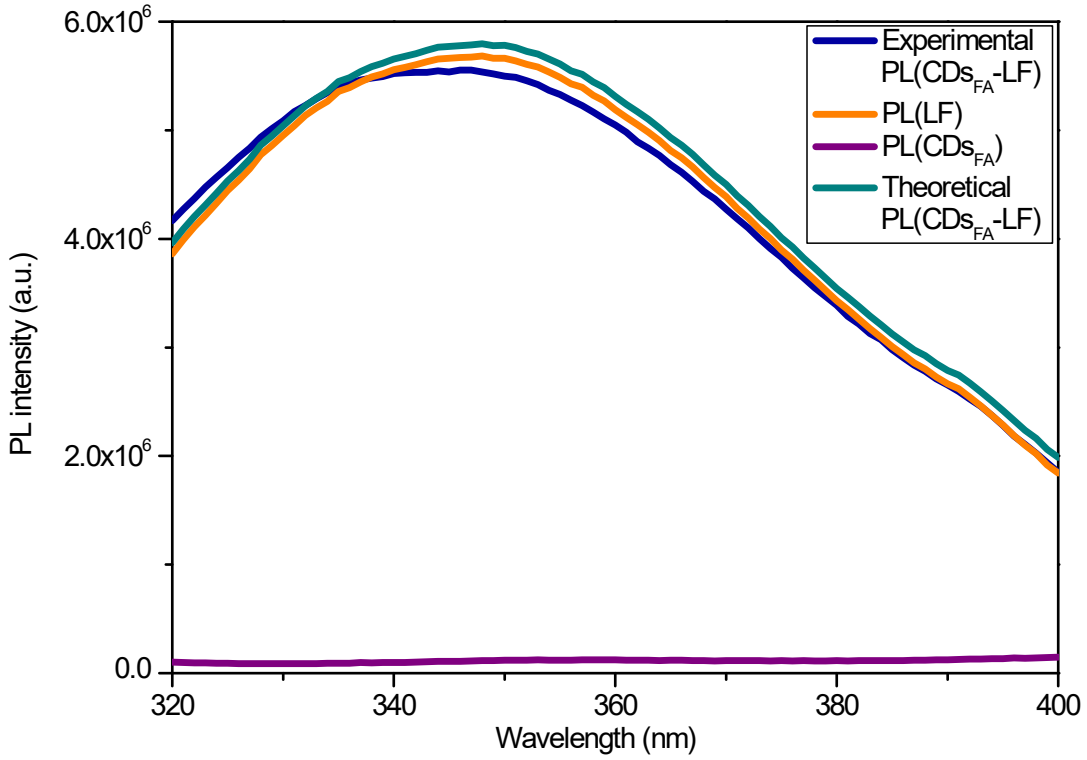

Fig. S12 Photoluminescence (PL) emission spectra of CDs_{FA} (purple), LF (orange), LF in the presence of CDs_{FA} (CDs_{FA}-LF; blue) and the theoretical sum of PL intensity of CDs_{FA} and LF (CDs_{FA}-LF; cyan). Experimental conditions: [LF] = 0.5 µM and [CDs_{FA}] = 2 µg/mL in a phosphate buffer 20 mM, pH 7.4 at 25 °C. λ_{exc} = 280 nm.

7. **CD_{FAs} structural and comparative data with Jin et *al.*' study.**

Jin *et al.* previously described the analogies they observed between Carbon dots they obtained from Folic Acid, CDs hereafter, and the starting material, FA.[3] Indeed, they proposed, that the pterin core, recognized by the FA-R, is conserved after hydrothermal synthesis of FA. These comparisons were performed using several analytical techniques: XPS, UV-visible, fluorescence spectroscopy, FT-IR and NMR.

We compared the nanoparticles obtained in the present study (CDs_{FA}) to the CDs synthesized by Jin *et al.* to try to identify structural similarities.

a) <u>XPS analysis</u>:

The XPS full-scale spectrum illustrated that CDs from Jin et *al.* are made of carbon (60.3%), nitrogen (18.7%), and oxygen (19.1%). Moreover, high-resolution spectra of C1s, N1s, and O1s

revealed especially the presence of –C=O,-C-O, -C-N, and -C=C (Table S2). As shown in Table S3, this composition is close to the one observed with CDs_{FA}.

Nature	C	N	O
Proportion	65,97%	17,95%	16,09%
Attribution (measured kinetic energy ; eV)	-C=O (288,7) -C-O/-C-N (285,8) -C=C/-C-C (284.7)	Pyridinic N (399.4)	-C=O (531.1)

Table S2 CDs XPS data from C1s, N1s and O1s spectra from Jin et *al*.

Nature	C	N	O
Proportion	60.3%	18.7%	19.1%
Attribution (measured kinetic energy ; eV)	-C=O (288.8) -C-O/-C-N (287.6) -C=C/-C-C (284.4, 285.5).	Pyridinic N: N-C and N-H (399.2)	-C-O and -C=O (531.0)

Table S3 CDs_{FA} XPS data from C1s, N1s and O1s spectra from the present study.

b) <u>UV-visible spectra</u>:

CDs_{FA} UV-visible spectrum shows the presence of two absorption bands at 274 nm, corresponding to the π→π* transition of para-aminobenzoic acid, and at 348 nm, corresponding to the n→π* transition of pterin ring. These bands are closed to the one announced by Jin *et al*. (280 nm, for the π→π* transition, and 320 nm, for the n→π* transition).

c) <u>Photoluminescent properties</u>:

The photoluminescent (PL) emission spectra indicated that the behavior of both CDs and CDs_{FA} is independent of the excitation wavelength for wavelengths ranging from 260 nm to 380 nm. Furthermore, the PL emission of CDs_{FA} is located at approximately 450 nm when excited at 360 nm while this maximum of PL emission is at 455 nm for the CDs.

d) <u>FTIR analysis</u>:

The absorbed bands present in CDs_{FA} spectrum at 3206, 1679 and 1404 cm^{-1} correspond to the fingerprints of their amine, carbonyl and alkene functions (Table S4) and can be associated with

the presence of pterin and aromatic moieties within them CDs_{FA}, as also proposed for CDs (Table S4).

	CDs from Jin et *al.*	CDs_{FA} in this study
Peaks (cm^{-1})	ν_{OH}: 3415 $\nu_{\text{-C-N, C=C}}$: 1485 (pterin and benzene)	$\nu_{OH/NH}$: 3206 $\nu_{\text{-C=O}}$: 1679 $\nu_{\text{-C-O,-C-N,C=C}}$: 1288 and 1404 (pterin et benzene)

Table S4 FTIR data from Jin et *al.* (left) and from the present study (right).

^{1}H NMR data:

Aromatic signals are provided in ^{1}H NMR spectrum of CDs_{FA} (Fig S13, bottom) and some of them could be assigned to the hydrogen atoms present in pterin and/or benzene rings found in FA's structure (Fig S13, top). The corresponding chemical shifts, in ppm, are located at 6.64, 7.65, and 8.65 ppm in ^{1}H NMR spectrum of CDs (Table S5).

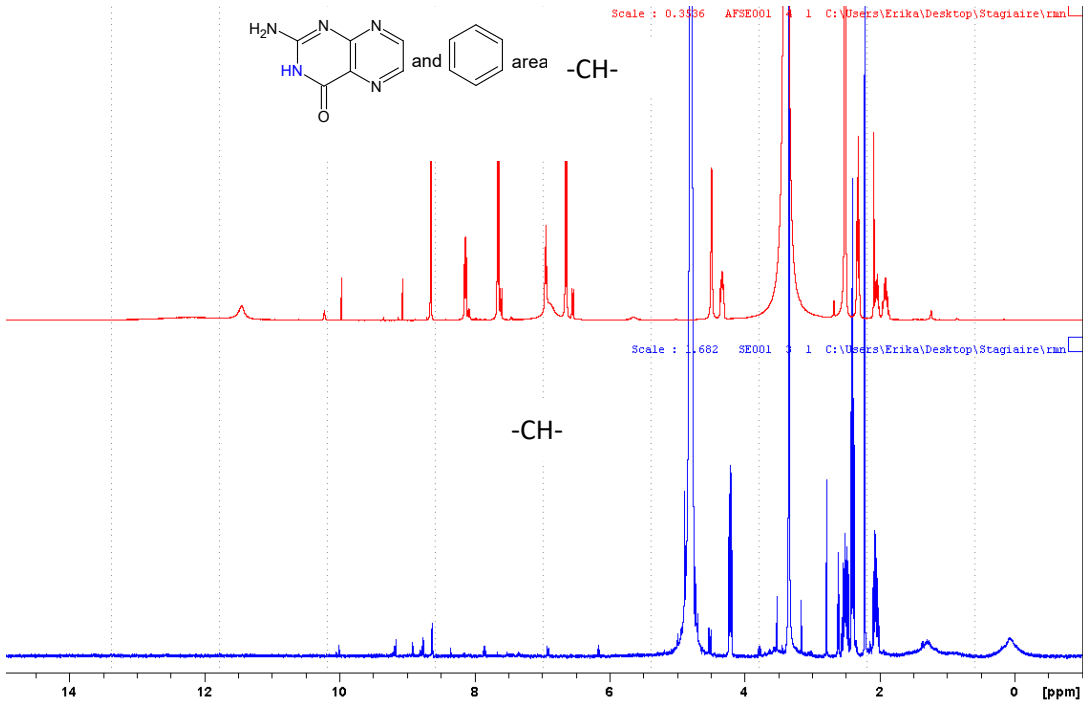

Fig. S13 ^{1}H NMR spectra of FA (red spectrum, top) and CDs_{FA} (blue spectrum, bottom) recorded in DMSO-d_6 and D_2O, respectively.

	CDs from Jin et *al.*	CDs_{FA} in this study
δ (ppm)	8.65, 7.65 and 6.64	8.63, 7.86 and 6.91
Attribution	Aromatic H	Aromatic H

Table S5 H^1 NMR data of CDs_{FA} from Jin et *al.* (left) the present study (right).

8. **References:**

1 M. Jorns and D. Pappas, A Review of Fluorescent Carbon Dots, Their Synthesis, Physical and Chemical Characteristics, and Applications, *Nanomaterials*, 2021, **11**, 1448.

2 T. H. L. Han, J.-M. Camadro, F. Barbault, R. Santos, J.-M. El Hage Chahine and N.-T. Ha-Duong, *Biochim. Biophys. Acta BBA - Gen. Subj.*, 2019, **1863**, 883–892.

3 Y. Jin, Q. Zhang, X. Qin, Z. Liu, Z. Li, X. Zhong, L. Xia, J. He and B. Fang, Carbon dots derived from folic acid attenuates osteoarthritis by protecting chondrocytes through NF-κB/MAPK pathway and reprogramming macrophages, *J. Nanobiotechnology*, 2022, **20**, 469.